Photochemistry of Aqueous C_{60} Clusters: Wavelength Dependency and Product Characterization

WEN-CHE HOU,*,†,⊥ LINGJUN KONG,‡,§ KEVIN A. WEPASNICK,|| RICHARD G. ZEPP,§ D. HOWARD FAIRBROTHER,|| AND CHAD T. JAFVERT*,†

School of Civil Engineering, Purdue University, West Lafayette, Indiana 47907, United States, National Research Council Associate, National Exposure Research Laboratory, Ecosystems Research Division, U.S. Environmental Protection Agency, Athens, Georgia 30605, United States, and Department of Chemistry, Johns Hopkins University, 3400 North Charles Street, Baltimore, Maryland 21218, United States

Received April 18, 2010. Revised manuscript received September 21, 2010. Accepted September 28, 2010.

To construct accurate risk assessment models for engineered nanomaterials, there is urgent need for information on the reactivity (or conversely, persistence) and transformation pathways of these materials in the natural environment. As an important step toward addressing this issue, we have characterized the products formed when aqueous C_{60} clusters (nC_{60}) are exposed to natural sunlight and also have assessed the wavelengths primarily responsible for phototransformation. Long-wavelength light ($\lambda \geq 400$ nm) isolated from sunlight, was shown to be important in both the phototransformation of nC_{60} and in the production of $^1O_2$. The significance of visible light in mediating the phototransformation of nC_{60} was supported by additional experiments with monochromatic light in which the apparent quantum yield at 436 nm ($\Phi_{436\ nm} = (2.08 \pm 0.08) \times 10^{-5}$) was comparable to that at 366 nm ($\Phi_{366\ nm} = (2.02 \pm 0.07) \times 10^{-5}$). LDI-TOF mass spectrometry indicated that most of the photoproducts formed after 947 h of irradiation in natural sunlight retain a 60 atom carbon structure. A combination of ^{13}C NMR analysis of ^{13}C-enriched nC_{60}, X-ray photoelectron spectroscopy and FTIR indicated that photoproducts have olefinic carbon atoms as well as a variety of oxygen-containing functional groups, including vinyl ether and carbonyl or carboxyl groups, whose presence destroys the native π-electron system of C_{60}. Thus, the photoreactivity of nC_{60} in sunlight leads to the formation of water-soluble C_{60} derivatives.

Introduction

Release of increasing quantities of carbon-based nanomaterials (CNMs), including C_{60}, to natural and engineered environments is inevitable due to the growing number of commercial products that contain CNMs. This has increased the urgency for research on the fate, transport, and persistence of CNMs in the environment (*1*). Previously, it has been shown that aqueous C_{60} clusters (nC_{60}) undergo phototransformation in sunlight (*2*) forming water-soluble products that have higher photoreactivity than the native nC_{60} colloidal suspensions, as measured by the singlet oxygen ($^1O_2$) production rate (*3*). The physicochemical properties of most functionalized C_{60} derivatives, including polyhydroxylated C_{60}, (i.e., fullerenol or fullerol) drastically deviate from those of underivatized C_{60}. Observed changes in environmentally relevant properties upon functionalization have included increased aqueous solubility (*4*); enhanced mobility in natural waters and through porous media (*5*); changes in toxicity (*6*); and altered production rates of reactive oxygen species (ROS) under UV irradiation (*7, 8*). Assessing potential health and safety effects of CNMs therefore requires detailed characterization of the products that form as a result of their exposure to the natural environment.

While the synthesis chemistry of C_{60} derivatives has received much attention (*9, 10*), information on the potential reactions of C_{60} in nature and in engineered systems is only now beginning to emerge. In engineered environments that mimic conditions present in water treatment plants, aqueous C_{60} clusters have been shown to react with ozone (*11*), and also transform under 254 nm UV light (*12*), in both cases forming water-soluble C_{60} products containing multiple hydroxyl and oxygen functionalities, similar to those of commercial fullerenols. Environmentally mediated transformations of oxygenated C_{60} molecules have also been reported. For example, Kong et al. (*8*) reported that fullerenol is extensively phototransformed to CO_2 upon exposure to simulated sunlight. Biologically mediated transformations of fullerenol also can occur; Schreiner et al. (*13*) reported that white rot basidiomycete, a soil-derived fungus, was capable of metabolizing ^{13}C-labeled fullerenol, in which the stable isotope ^{13}C from fullerenol was converted to CO_2 or incorporated into fungal biomass.

The focus of the present study is to assess the transformations of C_{60} that occur in the natural environment, specifically the photochemical effects of sunlight. Building on our earlier studies (*2, 3*), in which factors controlling the phototransformation kinetics of nC_{60} in sunlight were reported, herein we characterize the photoproducts by transmission electron microscopy (TEM), mass spectrometry, ^{13}C- nuclear magnetic resonance (NMR) spectroscopy, Fourier transform infrared (FTIR) spectroscopy, and X-ray photoelectron spectroscopy (XPS). Additionally, we have examined the wavelength dependency of phototransformation using 400- and 280-nm cutoff filters in sunlight, and by performing experiments with monochromatic light at 366 nm and at 436 nm within a photochemical reactor.

Materials and Methods

Materials. Sublimed C_{60} (99.9%) and ^{13}C-labeled (25% enriched) C_{60} (99+%) were purchased from the MER Corp. (Tucson, AZ). Other chemicals were of the highest purity available and used as received. All aqueous samples were prepared using water purified with a Barnstead Nanopure system (Dubuque, IA).

Preparation of nC_{60}. Aqueous C_{60} clusters were prepared either by a tetrahydrofuran (THF) transfer method (referred to as THF/nC_{60}) or by extended stirring of pulverized C_{60} in water (referred to as AQU/nC_{60}) following procedures similar to those described previously (*3*) and briefly reported in

* Address correspondence to either author. Phone: (765) 494-2196 (C. T. J.); (480) 727-9463 (W. C. H.). E-mail: jafvert@ecn.purdue.edu (C. T. J.); whou4@asu.edu (W. C. H.).
† Purdue University.
‡ National Research Council Associate.
§ Environmental Protection Agency.
|| Johns Hopkins University.
⊥ Current address: School of Sustainable Engineering and the Built Environment, Arizona State University, Tempe, Arizona 85287, United States.

10.1021/es101230q
Published on Web 10/12/2010

the Supporting Information (SI). In experiments where products were characterized by mass spectrometry, FTIR and XPS, AQU/nC_{60} solutions were used without added salts or buffers to avoid potential interferences by impurities. In experiments where samples were analyzed by ^{13}C NMR analysis, THF/nC_{60} was used because significantly less ^{13}C-enriched C_{60} was required for solution preparation.

Irradiation. All solar irradiations occurred either on the roof of the Civil Engineering Building at Purdue University (West Lafayette, IN, 86° 55′ W, 40° 26′ N) or on a nearby farm field where sunlight intensity was recorded. Due to the lengthy sunlight exposure time required to produce sufficient products, some experiments were performed in a glass-covered temperature-controlled (25 °C) greenhouse during winter months when the outside temperature was below 0 °C, with continued outdoor exposure once the weather warmed. More information on sample preparation, experimental procedures, and sunlight intensity data acquisition can be found in earlier publications (*2, 3*) and is briefly reported in the SI. In experiments that examined wavelength dependent effects, sample tubes were attached to the bottom of black boxes (5 cm in depth × 38 × 38 cm), on top of which 280 or 400 nm cutoff filters (Polycast UVT (280 nm cutoff) and UF-3 (400 nm cutoff), Spartech Corp., Clayton, MO) were clamped during exposure to sunlight.

Photoreaction quantum yield studies were performed in a rotating turntable reactor (i.e., a merry-go-round reactor (MGRR) *8, 14*), within which monochromatic light at 366 or 436 nm was isolated from a Hanovia mercury vapor lamp by a combination of Corning 0−52 and 7−37 glass filters or of Corning 3−73 and 5−58 glass filters, respectively. The temperature was maintained at 22 ± 1 °C using a NESLAB recirculating water bath. Monochromatic irradiation experiments were performed using 8 mL cylindrical Pyrex glass tubes (100 × 13 mm) filled with 5 mL of AQU/nC_{60} (1.5 mg/L) with an average particle size of 220 nm as measured by dynamic light scattering (DLS). All samples were prepared in triplicate. Dark control samples were prepared in identical glass tubes wrapped with aluminum foil. To determine the light intensity in MGRR experiments, potassium ferrioxalate (0.15 M in 0.1 N H_2SO_4), a chemical actinometer, was irradiated in parallel with samples at 366 or 436 nm in the MGRR. The detailed procedure was previously reported (*14*). The measured photon radiation intensity (I_λ) at 366 and 436 nm was 0.00724 and 0.00190 mol photon $L^{-1}\,h^{-1}$, respectively. The "apparent" quantum yield for photoreaction of nC_{60} at wavelength λ, ($(\Phi)_{nC60,\lambda}$), was calculated using eq 1 (*14*).

$$(\Phi_{nC_{60},\lambda}) = \frac{k_{\mathrm{obs},\lambda}}{2.303(I_\lambda)(\varepsilon_\lambda)(l)} \quad (1)$$

where $k_{\mathrm{obs},\lambda}$ is the pseudo first-order rate constant obtained for the photoreaction with monochromatic light (i.e., 0.0108 h^{-1} measured at 366 nm and 0.0023 h^{-1} measured at 436 nm), ε_λ is the molar absorption coefficient of AQU/nC_{60} at wavelength 366 and 436 nm, l is the light path length (1 cm), and I_λ (mol photon L^{-1} h^{-1}) is the radiation intensity determined using the ferrioxalate actinometer. In our case, the values we report for $(\Phi)_{nC60,\lambda}$ are "apparent" quantum yields since nC_{60} is a heterogeneous colloidal suspension rather than a homogeneous solution, leading to several complications in applying eq 1, with one of these being difficulty in accounting for light scattering, which in turn complicates precise measurement of molar absorption coefficients and the light path length. To help take into account the light scattering effect, the attenuation coefficients, scattering coefficients, and absorption coefficients of AQU/nC_{60} were measured using a SHIMADZU UV-2450 spectrophotometer equipped with an ISR-2200 integrating sphere attachment (60 mm in i.d. and with $BaSO_4$ inside coating). The spectra recorded with and without the integrating sphere are reported in Figure 1. The molar absorption coefficients determined using this instrument were 3.28 × 10^4 and 2.30 × 10^4 M^{-1} cm^{-1} at 366 and 436 nm, respectively. The scattering albedo, which is defined as the ratio of the scattering coefficient to the total attenuation coefficient (*15*) of the AQU/nC_{60}, was calculated to be ∼0.3 at these two wavelengths. Without specific indication, all other measurements of UV−visible spectra in this study were conducted using spectra obtained without the integrating sphere attachment (i.e., light attenuation). Within the nC_{60} clusters, surrounding C_{60} molecules are quite efficient in quenching the C_{60} excited state, significantly lowering $(\Phi)_{nC60,\lambda}$ compared to its values measured in homogeneous organic solvent solutions (2). Since we define $(\Phi)_{nC60,\lambda}$ as the photoreaction quantum yield (i.e., phototransformation of C_{60}), our reported values will be much less than that of triplet state production under the same conditions.

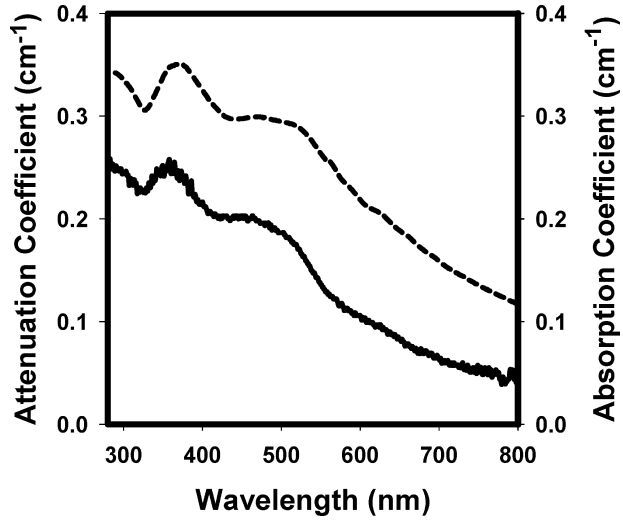

FIGURE 1. Comparison of attenuation coefficients (dashed line) and absorption coefficients (solid line) of AQU/nC_{60}. The absorption coefficients were measured using a SHIMADZU UV-2450 spectrophotometer equipped with an ISR-2200 integrating sphere attachment (60 mm in i.d. and with $BaSO_4$ inside coating).

To produce sufficient materials for product characterization, 43 mL aliquots of AQU/nC_{60} (2.2 L at 10 mg/L) were placed in a number of cylindrical borosilicate glass tubes (25 mm O.D. × 150 mm) and then exposed to sunlight for an extended length of time. All product characterization except for ^{13}C NMR analysis was performed on the material generated in these tubes. Most of the irradiated and dark control samples (2 L each) were concentrated by removing water in a rotary evaporator. The resulting ∼10 mL samples were vacuum-dried and the solid residues pulverized, and then heated in an oven at 70 °C for 4 days. The particles contained in the remaining volume of AQU/nC_{60} were analyzed by DLS, mass spectrometry, and TEM as described below.

Analysis. In wavelength-dependent experiments, the concentrations of furfuryl alcohol (FFA), used as a $^1O_2$ trapping reagent, and C_{60} were determined by HPLC with UV detection reported previously, with molecular C_{60} separated and detected by HPLC after removal from the aqueous phase by the reported (*2, 3*) or by an alternative method. By using the reported (*2, 3*) liquid−liquid extraction, complete (∼100%) recovery of C_{60} was attained from THF/nC_{60}. However, because we observed incomplete C_{60} recovery from irradiated AQU/nC_{60} by the cited method, C_{60} was recovered from the solutions by drying 1−2 mL samples under N_2 gas, and dissolving the residue in a double volume of toluene under mild sonication for ∼3 h prior to HPLC analysis of the

toluene phase. This increased the efficiency of C_{60} recovery to 69.3 ± 0.6% ($n = 3$) of the initial mass as compared to only 15.3 ± 1.1% recovery obtained by using the liquid−liquid extraction method prior to HPLC analysis. The DLS and TEM procedures have been described previously (*2*). Samples for TEM and mass spectrometry were concentrated seven times by drying under N_2 prior to analyses.

Matrix-assisted laser desorption ionization (MALDI) mass spectrometric results were obtained using an Applied Biosystems (Framingham, MA) Voyager DE PRO mass spectrometer. This instrument utilizes a nitrogen laser (337-nm laser) for ionization with a time-of-flight (TOF) mass analyzer. The positive ion mass spectra were obtained in the linear mode. The accelerating voltage was set at 20 kV and the grid voltage at 72%. The extraction delay time was set at 225 ns. The acquisition mass range for this study was 100−10 000 Da. There were 50 laser shots per spectrum. In samples where a matrix (i.e., α-cyano-4-hydroxycinnamic acid) was used, the sample and matrix were mixed in a ratio of 1:1 (v:v) on the sample plate. This mixture was allowed to air-dry prior to insertion into the mass spectrometer for analysis.

For XPS analysis, samples were prepared by dusting dry nC_{60} onto conductive double stick copper tape, such that no copper could be seen (typically ~3 mg). XP spectra were obtained with a PHI 5400 XPS system ($P_{base} < 5 \times 10^{-9}$ torr) using Mg Kα X-ray irradiation (1253.6 eV). Ejected photoelectrons were measured with a precision high energy electron analyzer operating at a constant pass-energy (44.75 eV) with a scan rate of 0.125 eV/step. XP spectra were processed with commercially available software (CasaXPS), and atomic concentrations were quantified by integration of the appropriate photoelectron peaks.

FTIR spectra were recorded on a Thermo Nicolet Nexus 670 FTIR spectrophotometer. Samples were prepared by embedding dried AQU/nC_{60} (0.67 mg) in KBr pellets (50 mg).

All NMR spectra were acquired at 20 °C on a Varian Inova 600 MHz spectrometer (599.7 MHz, ^{1}H) using a 5 mm broadband probe (Varian, Palo Alto, CA). All NMR samples were prepared by mixing ^{13}C-enriched (25%) THF/nC_{60} with 20% (v/v) D_2O in 5 mm standard NMR tubes. ^{13}C chemical shifts were referenced to tetramethylsilane (TMS). In all experiments, 102 400 transients were collected without ^{1}H decoupling using a 34.2 kHz spectral width, 2 s prescan delay and 1 s acquisition time. The data were processed using MestReC (MestreC Research, Santiago de Compostela, Spain) with 10 Hz apodization followed by zero-filling to 128 k points.

Results and Discussion

Wavelength Dependency. Figure 2a shows the results of C_{60} loss from THF/nC_{60} suspensions under the 280 and 400 nm cutoff filters from 10 a.m. to 4 p.m. on sunny or partly cloudy days in late October to early November sunlight. The 280 nm cutoff filter essentially acts as a control, as all wavelengths of solar irradiation (i.e., ≥ 300 nm) in the troposphere can pass through the 280 nm cutoff filter. The rate of C_{60} loss was ~40% less for samples irradiated through the 400 nm filter compared to the 280 nm filter, with the apparent first order rate constants equal to 0.034 and 0.054 h^{-1}, respectively. Since both filters transmit ~90% of the light above the respective cutoff wavelength as shown in SI Figure S1, this result suggests that long-wavelength solar irradiation (i.e., ≥ 400 nm) contributes significantly to C_{60} phototransformation when present as nC_{60}.

Photochemical reaction kinetics may be described by eq 2, where the transformation rate is a function of the radiation intensity, I_λ; the molar absorption coefficient of the chemical, ε_λ; the wavelength range (λ_b to λ_a) over which the chemical absorbs light; the light path length, l; and the quantum yield, Φ_λ:

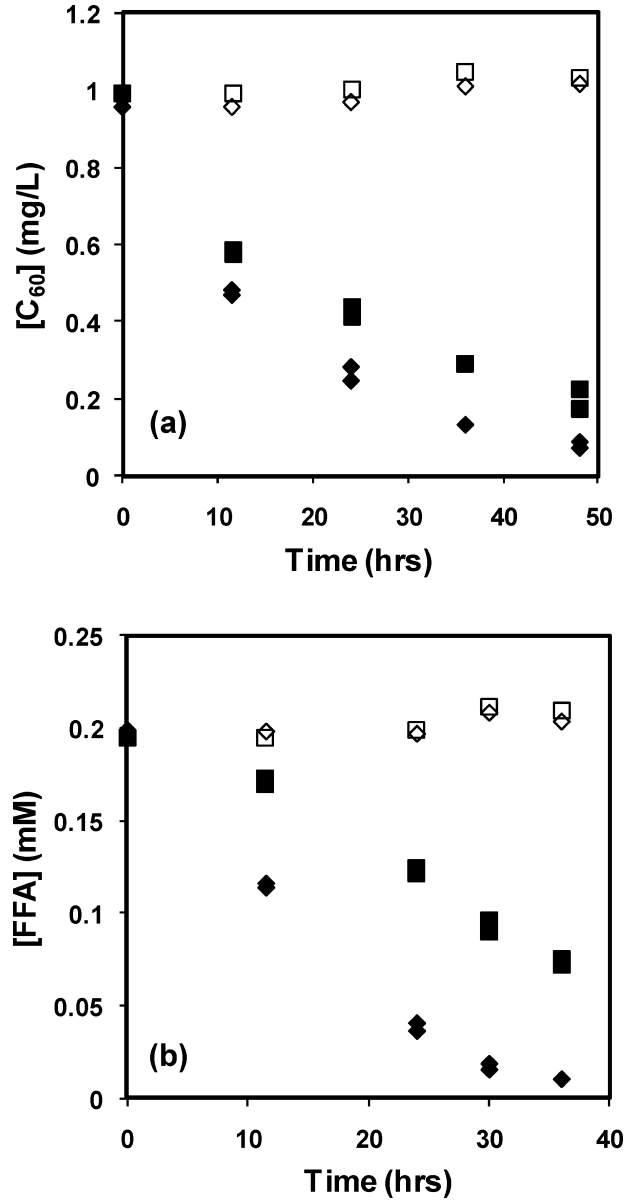

FIGURE 2. (a) Loss of C_{60} from solutions containing THF/nC_{60} (1 mg/L) under 280- (◆) and 400-nm (■) cutoff filters irradiated in sunlight at pH 7 from October 20 to November 2, 2008; and (b) decay of FFA (0.2 mM) in the present of 1 mg/L THF/nC_{60} under the same conditions. Open symbols are the corresponding dark control samples under the 280- (◇) and 400-nm (□) cutoff filters. The average solar irradiance from 300−800 nm during irradiation was 292 Wm^{-2}.

$$\frac{d[C]}{dt} = -\int_{\lambda_a}^{\lambda_b} I_\lambda \Phi_\lambda (1 - 10^{-\varepsilon_\lambda [C] l}) d\lambda \qquad (2)$$

Based on the absorption spectra of the nC_{60} suspensions that were measured using an instrument equipped with an integrating sphere to measure scattered light, the average fraction of light absorbed in the visible region (400−800 nm) is about one-half that at wavelengths <400 nm. Combined with the fact that the sunlight intensity (i.e., number of photons per area) at $\lambda > 400$ nm is ~7-fold higher than that at wavelength <400 nm (SI Figure S2), it is clear that visible light is responsible for a significant portion of nC_{60} phototransformation. The kinetic study using monochromatic light (SI Figure S3) further supports this view, as the apparent quantum yield ($\Phi_{nC60,\lambda}$), determined using eq 1 and measured at $\lambda = 436$ nm was (2.08 ± 0.08) × 10^{-5}, comparable to that at $\lambda = 366$ nm of (2.02 ± 0.07) × 10^{-5}. It should be noted that

although C_{60} clusters used for sunlight experiments under cutoff filters (THF/nC_{60}) and those used in monochromatic light studies (AQU/nC_{60}) are different, they qualitatively exhibit similar light absorption characteristics, with absorption bands at ~360 and 450−570 nm (SI Figure S2).

In a separate experiment (Figure 2b) where 1 mg/L THF/nC_{60} suspensions were irradiated under 280 or 400 nm cutoff filters with 0.2 mM FFA added as a $^1O_2$ trapping agent, a slightly higher FFA decay rate was obtained under the 280 nm cutoff filter consistent with the relative rate of C_{60} loss shown in Figure 2a. Especially under the 400 nm filter, FFA loss appears autocatalytic, consistent with our earlier study (*3*) where the soluble photoproducts were more photoreactive than the parent THF/nC_{60}.

Photoproduct Characterization. To prepare sufficient materials for product characterization, 2.2 L of AQU/nC_{60} (at 10 mg/L) was irradiated in sunlight from May 17 to August 16, 2009 (SI Figure S4) due to the lengthy irradiation time required to produce sufficient quantities of photoproducts. In sunlight, C_{60} loss occurred with an average first-order rate constant of 0.0042 h^{-1} whereas the dark control samples showed negligible loss (SI Figure S4a). The rate of C_{60} decay under these conditions was approximately 1 order of magnitude slower than that measured from Figure 2a (0.034 and 0.054 h^{-1}), primarily due to the higher optical density at 10 mg/L; however other factors likely contributed also, including sunlight intensity, weather, tube geometry, and nC_{60} particle size (*2*). After 947 h of sunlight exposure, the average particle size decreased from 330 to 170 nm as determined by DLS and confirmed by TEM imaging. Because C_{60} was undetectable on HPLC chromatograms after 947 h of sunlight exposure, the TEM image at 947 h (SI Figure S4b) is that of transformation products existing within smaller poly dispersed aggregates. The UV−visible absorbance spectrum of the irradiated sample shows significant decrease in the characteristic absorbance peaks of AQU/nC_{60} at 224, 284, and 360 nm, and significant decrease in a broad absorption band from 450−570 nm (SI Figure S4c). These results for AQU/nC_{60} under sunlight exposure are consistent with our previous results where THF/nC_{60} was exposed to lamp light within the solar spectrum ($\lambda = 300-410$ nm) (*2*).

Figure 3 shows mass spectra of samples derived from the same experiment reported on in SI Figure S4. The dark control sample (Figure 3a) shows the molecular ion peak at 720 m/z with minor peaks at 696 and 672 m/z (Figure 3a inset). The minor peaks can be attributed to C_{60} fragmentation during laser desorption ionization (LDI), as they became more pronounced if the laser energy is increased (not shown). The sample after 947 h of sunlight exposure (Figure 3b) shows a similar mass spectrum with the molecular ion peak at 720 m/z and slightly more fragmented molecular ions (i.e., m/z < 720). No significant spectral intensity was observed at m/z < 500. As the C_{60} concentration in the irradiated sample is below the detection limit, as measured by our extraction and HPLC method, the major peak at 720 m/z suggests that the oxygenated C_{60} products (see below) lose the oxygen-containing functionalities during LDI, resulting in the observed 60-carbon ion peak at 720 m/z. Indeed, we have not observed molecular ions at m/z > 720, where oxygenated C_{60} derivatives should exist if detectable, consistent with mass spectra result of polyhydroxylated C_{60} (*9, 11, 16*). For the irradiated sample, minor peaks from m/z = 512 to 648 were observed. These new species are generally spaced at 12, 16, or 24 amu increments (Figure 3b inset) and may be nonparent ion fragments of the fragile oxygenated 60-carbon atom products, fragmented during LDI (*17*), with the 16 Da mass differences suggesting some incorporation of oxygen moieties. Even if the peaks at m/z < 720 are primary molecular ions (in which case the 60-carbon structure is not maintained in sunlight) the predominance of the peak at m/z = 720

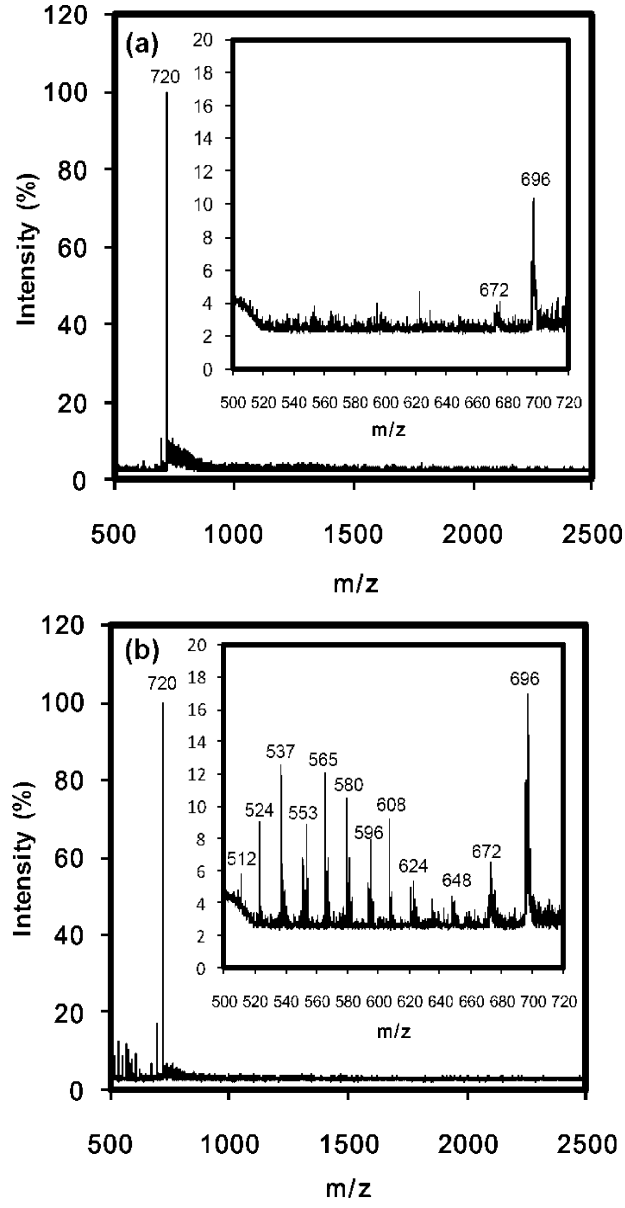

FIGURE 3. LDI-TOF mass spectroscopy of AQU/nC_{60}, showing (a) the dark control sample, and (b) the irradiated sample after 947 h.

indicates that the vast majority of product species retain the C_{60} structure. The use of α-cyano-4-hydroxycinnamic acid as a matrix to protect the analytes from fragmentation during ionization (i.e., MALDI) results in very similar mass spectra (not shown). This supports our assertion that most of the C_{60} photoproducts retain a 60-carbon structure, although the MS analysis also highlights the limitations of MS for product analysis in the case of C_{60} due to the facile fragmentation of the product species.

The effects of sunlight irradiation on the chemical composition of the same AQU/nC_{60} samples, probed using XPS, are shown in Figure 4. XP spectra of the C(1s) and O(1_S) regions are shown for three samples: (a) "as-received" (AR) C_{60} material from the manufacturer, (b) dark control samples, and (c) samples exposed to sunlight for 947 h. The AQU/nC_{60} samples reported in Figure 4b and c were suspended in water for approximately the same time period, and are the same as those reported on in Figure 3 and SI Figure S4. Thus, any differences in the chemical composition between Figures 4b and c can be ascribed solely to the effects of sunlight irradiation. The C(1s) region of the AR C_{60} (Figure 4a) is

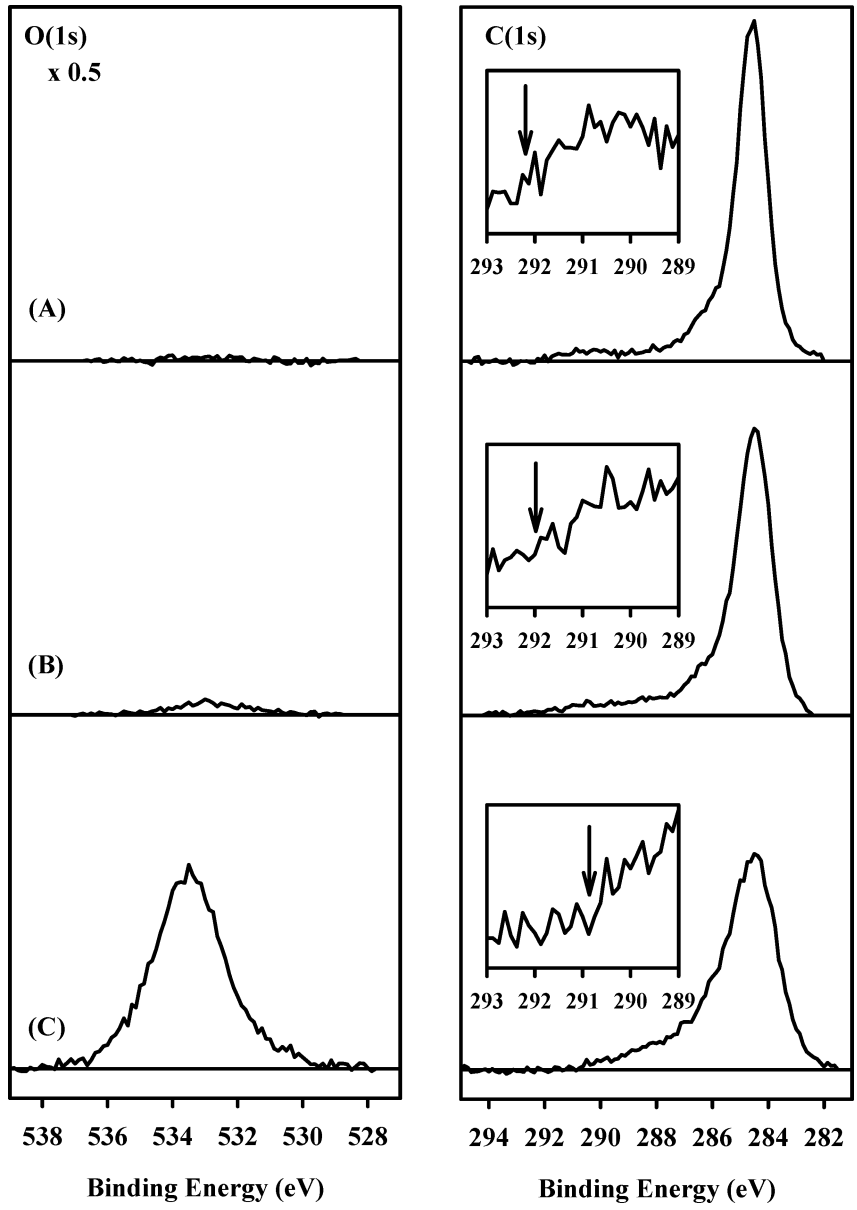

FIGURE 4. XP spectral envelopes of the O(1s) and C(1s) regions for (a) as-received C_{60}, (b) dark control AQU/nC_{60}, and (c) AQU/nC_{60} irradiated in sunlight for 947 h. For each sample, the integrated area under the C(1s) spectral envelope has been normalized and the O(1s) signal intensity adjusted accordingly. In the C(1s) spectra of (b), the binding energy regions for C—C/C=C and oxidized carbon atoms (i.e., CO_x species) has been shown. The inset in the C(1s) region shows the change in the $\pi-\pi^*$ shakeup feature centered at 291 eV for each C_{60} sample; in each insert, the vertical arrow indicates the binding energy below which spectral intensity is observed.

dominated by a single peak at a binding energy of 284.5 eV, whereas the O(1s) region is devoid of any spectral intensity. These observations are consistent with the chemical formula and structure of C_{60} and other XPS spectra of C_{60} (*18, 19*). In Figure 4a, a $\pi-\pi^*$ shakeup feature also can be discerned at ~291 eV in the C(1s) region (see insert); this feature arises from the simultaneous excitation of π electrons during the ejection of C(1s) photoelectrons and is evidence of a deconjugated π electron system in the AR C_{60}. For the control experiment in which AQU/nC_{60} samples were *not* exposed to sunlight, the C(1s) and O(1s) regions are largely unchanged compared to (a), with a dominant peak in the C(1s) region at 284.5 eV and virtually no signal intensity in the O(1s) region. Although there is a slight broadening of the C(1s) region to higher binding energies in dark control AQU/nC_{60} relative to the AR C_{60} (compare the C(1s) regions in Figure 4a and b), evidence of a $\pi-\pi^*$ shakeup feature can still be seen in the insert by virtue of the onset in spectral intensity at approximately 292 eV. Upon exposure of the AQU/nC_{60} samples to sunlight irradiation, significant changes are observed in both the C(1s) and O(1s) regions. Specifically, the C(1s) region broadens to higher binding energies and the peak at 284.5 eV becomes less dominant; in the O(1s) region there is a marked increase in spectral intensity. All of these changes are consistent with the effects that would be expected to accompany the oxidation of carbon atoms in the AQU/nC_{60} samples due to sunlight irradiation. Furthermore, the inset in the C(1s) region of Figure 4c exhibits no evidence of a $\pi-\pi^*$ shakeup feature; indeed, the onset of spectral intensity in the C(1s) region does not occur until below 291 eV, the peak position associated with the $\pi-\pi^*$ shakeup feature. Thus, XPS results indicate that photo-oxidation of AQU/nC_{60} samples leads to the formation of oxygen-containing functional groups and the destruction of the deconjugated π-electron system associated with the parent AQU/nC_{60}.

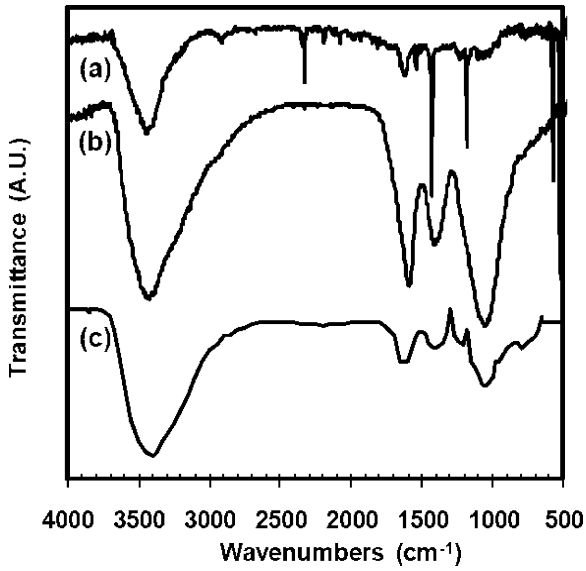

FIGURE 5. FTIR spectra of AQU/nC_{60} showing (a) the dark control sample, (b) the irradiated sample (947 h), and (c) a commercial fullerenol ($C_{60}(O)_x(OH)_y$, where $x + y = 22$) spectrum adapted from ref 11.

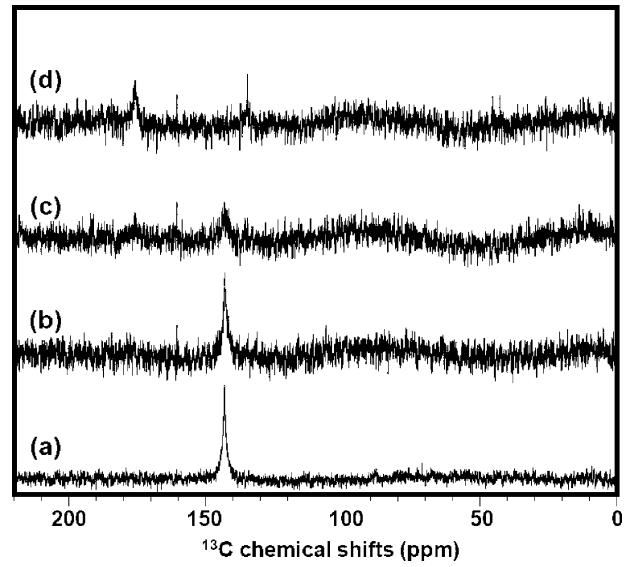

FIGURE 6. ^{13}C NMR spectra of ^{13}C-enriched (25%) THF/nC_{60} (58 mg/L) exposed to sunlight from February 12 to June 15, 2009, showing (a) a dark control sample, and samples after (b) 292 h, (c) 557 h, and (d) 1453 h of sunlight exposure. The remaining concentrations of C_{60} corresponding to spectra (b), (c), and (d) were 25, 5, and 0 mg/L, respectively.

The FTIR spectra of the irradiated (947 h) and the dark control AQU/nC_{60} samples generated from the experiment reported in Figures 3 and 4 and SI Figure S4 are presented in Figure 5. In each spectrum, the presence of a broad IR feature centered at approximately 3400 cm^{-1} can be attributed to water that was not removed during sample drying, or due to the moisture associated with the KBr pellets. The same peak also occurs in the AR C_{60} (not shown). In the dark control AQU/nC_{60} sample (Figure 5a), four sharp absorption peaks at 528, 577, 1183, and 1429 cm^{-1} are characteristic of pristine C_{60} (*20*). Other peaks at 1538, 1600, 2188, and 2326 cm^{-1} may be attributed to impurities in the AR C_{60} material (*20*) and/or in the KBr pellets, as these peaks are present also in the AR C_{60} (not shown). For the irradiated sample (Figure 5b), the characteristically sharp peaks of pristine C_{60} completely disappear and new broad absorption bands centered at 1060, 1390, and 1600 cm^{-1} appear. These new features are assigned as shown in SI Table S1, and are consistent with carbon−oxygen bonds. A comparison of Figure 5b and c reveals that the features of the irradiated AQU/nC_{60} sample (Figure 5b) closely resemble those of a commercial fullerenol ($C_{60}(O)_x(OH)_y$, where $x + y = 22$, (MER Corp.)) (Figure 5c) (*11*).

In a separate experiment where ^{13}C-enriched (25%) THF/nC_{60} (58 mg/L) was exposed to sunlight from February 12 to June 15, 2009, the ^{13}C chemical shift was recorded and reported in Figure 6. The dark control sample shows a single peak at 143 ppm (Figure 6a), which is 3 ppm upfield from previous reports on aqueous C_{60} clusters (*11, 21*), but is consistent with pristine C_{60} in the solid state (*22*) or dissolved in organic solvents (*23*). Upon sunlight irradiation, the peak at 143 ppm gradually decreased as C_{60} was lost from the aqueous suspensions with complete loss of the peak at 143 ppm coinciding with complete loss of C_{60} as measured by HPLC. In parallel, ^{13}C signals at 135, 161, and 176 ppm increased (Figure 6b−d), corresponding to olefinic carbons (C═C at 135 ppm) (*9*); vinyl ether carbon (C═C−O at 161 ppm) (*11, 13*); and carboxyl or carbonyl carbon (O = C−O or C═O at 176 ppm) (*11, 13, 24*).

Influence of Oxidizing Conditions on the Transformations of nC_{60}. Although the focus of this investigation was to characterize the photoproducts formed when nC_{60} is exposed to sunlight, it is useful to consider the similarities and differences between the results reported herein to results of other studies conducted under oxidizing conditions likely to be encountered in water treatment plants (i.e., $\lambda = 254$ nm and reaction with ozone) (*11, 12*). Whereas ozone reacts with nC_{60} within hours, photochemical reactions are slower, requiring days under UVC light (i.e., $\lambda = 254$ nm), and weeks or months under sunlight. In all three cases, the characteristic UV−visible light attenuation of nC_{60} at 220, 280, 360, and 500 nm decreases with time, as does the size of the nC_{60} particles. Irrespective of if nC_{60} particles are exposed to O_3, UVC light, or natural sunlight, the mass spectra indicate that most products retain the 60 carbon structure. FTIR spectra of the resulting products show analogous absorption characteristics with varied relative abundances. In particular, the peak at 1600 cm^{-1}, likely associated with carbonyl or carboxylate species, is significantly greater in intensity for O_3-treated nC_{60} than for UVB or UVC irradiated nC_{60}, suggesting more facile production of highly oxygenated species under O_3 treatment, although longer irradiation in natural sunlight likely would produce the same result. ^{13}C NMR spectra also indicate similar oxygenated products occur when nC_{60} is subjected to reaction with either ozone or sunlight. XPS results indicate that the extent of oxidation is noticeably higher for the reaction with O_3, with a larger fraction of C═O/O−C−O species. In summary, products formed within the different oxidizing environments show many similarities, with oxidation reactions occurring at a much slower rate in natural sunlight.

Acknowledgments

Financial support was provided by the United States Environmental Protection Agency (U.S. EPA) under Award RD 83334001 of the STAR grant program. We thank Dr. Changhe Xiao for technical assistance; Dr. Karl Wood at the campus-wide Mass Spectrometry Center (CWMSC) of Purdue University for mass spectrometric analysis and discussion; Ms. Debra Sherman at the Life Science Microscopy Facility of Purdue University for TEM imaging; Prof. Hugh Hillhouse and Dr. Qijie Guo at the School of Chemical Engineering of Purdue University for use of the FTIR spectrophotometer and help in recording spectra; Dr. Zhengwei Pan and Mr. Yen-Jun Chuang at University of Georgia for transmittance/absorbance measurements using the UV−visible spectrometer equipped with an integrating sphere attachment; Drs. Quincy Teng and Wenlin Huang at the U.S. EPA, National

Exposure Research Laboratory, Athens, Georgia for ^{13}C NMR analysis and discussion. D.H.F. and K.W. gratefully acknowledge partial financial support from the National Science Foundation (Grant No. BES0731147), the Environmental Protection Agency (Grant No. RD-83385701-0) and the Institute for Nanobiotechnology at Johns Hopkins University. This paper has been reviewed in accordance with the U.S. EPA's peer and administrative review policies and approved for publication. Mention of trade names or commercial products does not constitute an endorsement or recommendation for use by the U.S. EPA.

Supporting Information Available

Additional information on light transmission of the filters; the UV−visible spectrum of THF/nC_{60} and AQU/nC_{60} and the solar spectrum; the kinetic study using monochromatic light; sunlight-irradiated AQU/nC_{60} decay kinetics and associated sample TEM images and UV−visible spectra; and a summary table of FTIR functionality assignment; discussion on the potential reaction pathways is provided. This material is available free of charge via the Internet at http://pubs.acs.org.

Literature Cited

(1) Wiesner, M. R.; Lowry, G. V.; Alvarez, P.; Dionysiou, D.; Biswas, P. Assessing the risks of manufactured nanomaterials. *Environ. Sci. Technol.* **2006**, *40*, 4336–4345.

(2) Hou, W.-C.; Jafvert, C. T. Photochemical transformation of aqueous C_{60} clusters in sunlight. *Environ. Sci. Technol.* **2009**, *43*, 362–367.

(3) Hou, W.-C.; Jafvert, C. T. Photochemistry aqueous C_{60} clusters: Evidence of $1O_2$ formation and its role in mediating C_{60} phototransformation. *Environ. Sci. Technol.* **2009**, *43*, 5257–5262.

(4) Jafvert, C. T.; Kulkarni, P. P. Buckminsterfullerene's (C_{60}) octanol-water partition coefficient (K_{ow}) and aqueous solubility. *Environ. Sci. Technol.* **2008**, *42*, 5945–5950.

(5) Lecoanet, H. F.; Bottero, J.; Wiesner, M. R. Laboratory assessment of the mobility of nanomaterials in porous media. *Environ. Sci. Technol.* **2004**, *38*, 5164–5169.

(6) Sayes, C. M.; Fortner, J. D.; Guo, W.; Lyon, D.; Boyd, A. M.; Ausman, K. D.; Tao, Y. J.; Sitharamen, B.; Wilson, L. J.; Hughes, J. B.; West, J. L.; Colvin, V. L. The differential cytotoxicity of water-soluble fullerenes. *Nano Lett.* **2004**, *4*, 1881–1887.

(7) Hotze, E. M.; Labille, J.; Alvarez, P.; Wiesner, M. R. Mechanisms of photochemistry and reactive oxygen production by fullerene suspensions in water. *Environ. Sci. Technol.* **2008**, *42*, 4175–4180.

(8) Kong, L.; Tedrow, O.; Chan, Y. F.; Zepp, R. G. Light-induced transformation of fullerenol in aqueous media. *Environ. Sci. Technol.* **2009**, *43*, 9155–9160.

(9) Chiang, L. Y.; Upasani, R. B.; Swirczewski, J. W.; Soled, S. Evidence of hemiketal incorporated in the structure if fullerols derived from aqueous acid chemistry. *J. Am. Chem. Soc.* **1993**, *115*, 5453–5457.

(10) Taylor, R.; Walton, D. R. M. The chemistry of fullerenes. *Nature* **1993**, *363*, 685–693.

(11) Fortner, J. D.; Kim, D. I.; Boyd, A. M.; Falkner, J. C.; Moran, S.; Colvin, V. L.; Hughes, J. B.; Kim, J.-H. Reaction of water-stable C_{60} aggregates with ozone. *Environ. Sci. Technol.* **2007**, *41*, 7497–7502.

(12) Lee, J.; Cho, M.; Fortner, J. D.; Hughes, J. B.; Kim, J.-H. Transformation of aggregates C_{60} in the aqueous phase by UV irradiation. *Environ. Sci. Technol.* **2009**, *43*, 4878–4883.

(13) Schreiner, K. M.; Filley, T. R.; Blanchette, R. A.; Bowen, B. B.; Bolskar, R. D.; Hockaday, W. C.; Masiello, C. A.; Raebiger, J. W. White-rot basidiomycete-mediated decomposition of C_{60} fullerol. *Environ. Sci. Technol.* **2009**, *43*, 3162–3168.

(14) Zepp, R. G.; Gumz, M. M.; Miller, W. L.; Gao, H. Photoreaction of valerophenone in aqueous solution. *J. Phys. Chem. A* **1998**, *102*, 5716–5723.

(15) Li Puma, G.; Brucato, A. Dimensionless analysis of slurry photocatalytic reactors using two-flux and six-flux radiation absorption-scattering models. *Catal. Today* **2007**, *122*, 78−90.

(16) Kokubo, K.; Matsubayashi, K.; Tategaki, H.; Takada, H.; Oshima, T. Facile synthesis of highly water-soluble fullerenes more than half-covered by hydroxyl groups. *ACS Nano* **2008**, *2*, 327–333.

(17) Deng, J.-P.; Ju, D.-D.; Her, G.-R.; Mou, C.-Y.; Chen, C.-J.; Lin, Y.-Y.; Han, C.-C. Odd-numbered fullerene fragment ions from C_{60} oxides. *J. Phys. Chem.* **1993**, *97*, 11575–11577.

(18) Onoe, J.; Nakao, A.; Takeuchi, K. XPS study of a photopolymerized C_{60} film. *Phys. Rev. B* **1997**, *55*, 10051–10056.

(19) Andreas, A. A.; Chang, W.; Lee, J. K. Effect of fullerene coating on silicon thin film anodes for lithium rechargeable batteries. *J. Solid State Elelctr.* **2010**, *14*, 51–56.

(20) Kratschmer, W.; Lamb, L. D.; Fostiropoulos, K.; Huffman, R. D. Solid C_{60}: A new form of carbon. *Nature* **1990**, *347*, 354–358.

(21) Fortner, J. D.; Lyon, D. Y.; Sayes, C. M.; Boyd, A. M.; Falkner, J. C.; Hotze, E. M.; Alemany, L. B.; Tao, Y. J.; Guo, W.; Ausman, K. D.; Colvin, V. L.; Hughes, J. B. C_{60} in water: nanocrystal formation and microbial response. *Environ. Sci. Technol.* **2005**, *39*, 4307–4316.

(22) Yannoni, C. S.; Johnson, R. D.; Meijer, G.; Bethune, D. S.; Salem, J. R. C-13 NMR study of the C_{60} cluster in the solid-state-molecular-motion and carbon chemical-shift anisotrophy. *J. Phys. Chem.* **1991**, *95*, 9–10.

(23) Taylor, R.; Hare, J. P.; Abdul-Sada, A. K.; Kroto, H. W. Isolation, separation and characterization of the fullerenes C_{60} and C_{70}: the third form of carbon. *J. Chem. Soc. Chem. Commun.* **1990**, 1423–1425.

(24) Lambert, J. B.; Shurvell, H. F.; Lightner, D. A.; Cooks, R. G. *Organic Structural Spectroscopy*; Prentice Hall: Upper Saddle River, NJ, 1998.

ES101230Q